Effectiveness of Co intercalation between Graphene and Ir(111)

Article *in* Chemical Physics Letters · February 2018

DOI: 10.1016/j.cplett.2018.02.054

7 authors, including:

Ilaria Carlomagno
Università Degli Studi Roma Tre
7 PUBLICATIONS **14** CITATIONS
SEE PROFILE

Jakub Drnec
European Synchrotron Radiation Facility
46 PUBLICATIONS **172** CITATIONS
SEE PROFILE

Andrea Maria Scaparro
Università Degli Studi Roma Tre
3 PUBLICATIONS **4** CITATIONS
SEE PROFILE

Roberto Felici
C.N.R. - Italian National Research Council
175 PUBLICATIONS **1,926** CITATIONS
SEE PROFILE

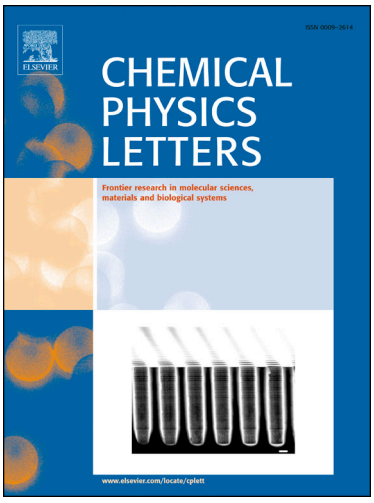

Effectiveness of Co intercalation between Graphene and Ir(111)

I. Carlomagno, J. Drnec, A.M. Scaparro, S. Cicia, S. Mobilio, R. Felici, C. Meneghini

PII: S0009-2614(18)30139-8
DOI: https://doi.org/10.1016/j.cplett.2018.02.054
Reference: CPLETT 35466

To appear in: *Chemical Physics Letters*

Received Date: 16 November 2017
Accepted Date: 19 February 2018

Please cite this article as: I. Carlomagno, J. Drnec, A.M. Scaparro, S. Cicia, S. Mobilio, R. Felici, C. Meneghini, Effectiveness of Co intercalation between Graphene and Ir(111), *Chemical Physics Letters* (2018), doi: https://doi.org/10.1016/j.cplett.2018.02.054

Effectiveness of Co intercalation between Graphene and Ir(111)

I. Carlomagno[1,*], J. Drnec[c], A. M. Scaparro[1], S. Cicia[1], S. Mobilio[1], R. Felici[b], C. Meneghini[1]

[a]*Dipartimento di Scienze, Università Roma Tre, Via della Vasca Navale 84, 00146 Rome - Italy*
[b]*CNR-SPIN, Area della Ricerca di Tor Vergata, Via del Fosso del Cavaliere, 100, 00133 Rome - Italy*
[c]*ESRF, 71 Avenue des Martyrs, 38000 Grenoble - France*

Abstract

Graphene can be used to avoid the oxidation of metallic films. This work explores the effectiveness of such stabilizing effect on Cobalt films intercalated between Graphene and Ir(111). After intercalation at 300 °C, two Co films are exposed to ambient pressure and investigated using Co-K edge X-ray Absorption Near Edge Spectroscopy. The formation of a disordered oxide phase is observed, and associated to the presence of some non-intercalated Co. Further annealing at 500 °C causes the oxide reduction to metallic Co which further intercalates below the Graphene. Once the intercalation is completed, Graphene prevents the Co from oxidation under ambient pressure conditions.

1. Introduction

Among their unique and promising properties, graphene (Gr) has an exceptional chemical stability which can be used to passivate highly reactive surfaces [1, 2]. This is a valuable benefit for thin films presenting perpendicular magnetic anisotropy (PMA) that, once stabilized against oxidation, become suitable candidates to develop ultra-high density magnetic recording devices [3, 4].

Large-area high-quality epitaxial Gr can be grown via chemical vapor deposition (CVD) [5, 6] on transition metal substrates. On Ir(111), CVD growth of Gr has been successfully performed in a range of growth temperatures from 600 to 1000 °C [7]. Thin films intercalation below Gr on Ir(111) has already been proven effective against deterioration for several systems [8, 9, 10, 11,

*Corresponding author. E-mail: ilaria.carlomagno@uniroma3.it (Ilaria Carlomagno)

12, 13]: among these, intercalated Co films (Gr/Co/Ir) have raised particular interest [14, 15, 16, 17, 18, 19, 20, 21] due to an unexpected PMA enhancement with respect to bare Co films grown on Ir(111) [22].

This work explores the thickness-dependent efficiency of the Co intercalation and the effects of air exposure at ambient pressure on Co films intercalated between Gr and Ir(111). By exploiting the chemical selectivity and the sensitivity to the coordination chemistry of X-ray Absorption Fine Structure (XAFS) spectroscopy, the stability of the film against oxidation is probed. The amount of oxidised Co is then used to evaluate the intercalation effectiveness. A thermal method for the Co oxide reduction is described. This method induces also the final intercalation of Co which becomes protected against further oxidation.

2. Experimental

The Gr/Co/Ir samples were prepared in the UHV chamber available at the ID03 preparation laboratory (ESRF - Grenoble, France), at a base pressure of 10^{-10} mbar, following a well established procedure [19, 21]. The Ir(111) substrate was cleaned through several cycles of Ar^+ sputtering at 1 kV, and thermal annealing at 850 °C. The surface quality was inspected by X-ray Photoelectron Spectroscopy (XPS), and Low Energy Electron Diffraction (LEED). The substrate was considered clean when XPS showed no contaminants peaks, and well defined, high-contrast LEED patterns were observed (Fig.S1*a*).

Gr was grown on clean Ir(111) by heating the substrate to 600 °C, and exposing it to $P = 10^{-7}$mbar of ethylene for 40 min. The C_2H_4 was then pumped out and the sample was slowly cooled down to room temperature (RT). The blurred, incomplete rings around the Ir spots in the LEED pattern (Fig.S1*b*) confirm the presence of defective Gr on the surface, suitable for low temperature (300 °C) Co intercalation [7, 13].

Two Co films of 10 ± 1 and 5 ± 1 monolayers (ML) were deposited on Gr/Ir at RT from an ultra-pure Co rod using an electron bombardment evaporator. The ratio of Co_{2p}/Ir_{4f} XPS peaks, collected with an exit angle of 45° to minimize morphology effects [23], was used to evaluate the films thickness [24]. The thickness was evaluated after the 300 °C annealing, as this treatment was

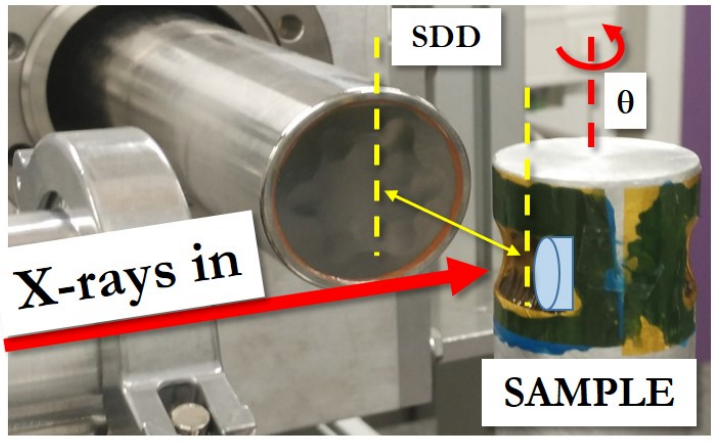

Figure 1: Experimental set-up used for XAFS measurements at the BM23 beamline, ESRF. The sample was placed in a vacuum chamber with Kapton windows with its surface vertical. The chamber was mounted on a rotating support allowing to vary the angle between the incoming beam and the sample surface. The detector was placed at 90° with respect to the X-ray beam and at ≃ 2 cm from the sample surface.

proven to reduce the surface and interface roughness of the film [19]. The error bars were estimated taking into account the experimental error and the uncertainty originated from the roughness effects [23]. The films intercalation was triggered by keeping each substrate at $T = 300 \pm 20$ °C for 5 min. The decreasing Co_{2p} XPS peaks, combined with the increasing C_{1s} peak (shown in Fig.S1), are interpreted as a sign of the agreement with previously reported intercalation protocols [13, 19].

Each intercalated film was exposed to ambient pressure for about 15 min. Then, it was loaded into the vacuum chamber (base pressure around 10^{-5} mbar) available at the BM23 beamline (ESRF, Grenoble) for XAFS measurements. Co K-edge XAS spectra were collected in fluorescence geometry in the near edge (XANES) region using a 13-elements Ge array detector (Canberra) placed at about 2 cm from the sample surface (Fig.1). The incident x-ray flux I_0, was measured using a gas filled ionization chamber. Data were acquired with the X-ray linear polarization closely perpendicular, ≃ 80° (parallel, ≃ 10°) to the sample surface in order to maximize the XAFS sensitivity to the structural features oriented perpendicular (parallel) to the film plane [25]. The Co K_α fluorescence signal I_f, was selected using the multi-channel analyser (MCA)

electronics of the detector. The live time was kept higher than 90% to keep non-linear effects negligible. The absorption signal was calculated as $\mu(E) = I_f/I_0$, neglecting the self absorption effects [25]. Several spectra were collected after tilting each sample by few centidegrees within ±0.1°: this resulted in a progressive energy shift of the Ir Bragg peaks which could be easily identified and removed from every spectrum acquired by each detector element [26, 27]. The XAS spectra were then averaged and normalized using standard procedures for X-ray absorption fine structure data treatment [25]. The Co edge energy (E_0) was selected at the first inflection point of the absorption coefficient measured from a Co reference foil.

The samples were then annealed in UHV for 5 min at 500°C and, after cooling down to room temperature, they were exposed again at ambient pressure for about 15 min. New spectra, $\mu_{\parallel,\perp}^{500C}(E)$, were then collected following the same procedure described above.

3. Results and discussion

The spectra collected after the first, $\mu_{\parallel,\perp}^{300C}(E)$, and the second annealing treatment, $\mu_{\parallel,\perp}^{500C}(E)$, are shown in Fig.2a and b for the thick and thin film, respectively. At the bottom of every panel, the difference $\Delta\mu(E) = \mu^{500C}(E) - \mu^{300C}(E)$ is reported for each polarization to facilitate the identification of the thermally-induced modifications.

Upon annealing and further air exposure, the two samples undergo a similar evolution and two major changes (labels A and B in Fig.2) emerge in the first 20 eV from the edge. Both the increase in the pre-edge shoulder (A, around 5 eV above the edge), and the reduced intensity of the white line (B, around 15-20 eV above the edge) stand out more clearly in the thick film data. At the bottom of every panel, the difference $\Delta\mu(E) = \mu^{500C}(E) - \mu^{300C}(E)$ is reported for each polarization to facilitate the identification of the thermally-induced modifications.

Comparing the XANES features of a sample with those of reference compounds is a reliable way to understand the coordination chemistry of the absorber and eventual multi-phase composition of the sample [28]. To this aim we collected a number of Co K edge XANES spectra in the same conditions and in the same experimental run. Our reference compounds were chosen to be: metallic Co, CoO, Co_3O_4 and Co_{aq} (Fig.S2). The latter was collected on Co^{2+} ions in aqueous solution, as a model for highly disordered Co oxide structure in which the next neighbors

coordination shells give negligible contributions to the XANES features.

XANES spectra collected after the 300 °C annealing (Fig.2) are compatible with the shape of the CoO and Co_{aq} spectra (Fig. S2), and are most likely due to the presence of an oxidised phase being suppressed by the 500 °C annealing. In order to identify the oxide type and to quantify its amount, we used a linear combination analysis (LCA) on both samples [28]. The experimental data $\mu^{300C}_{\perp,\parallel}(E)$ were fitted using a μ^{th} curve calculated as:

$$\mu^{th}_{\parallel,\perp}(E) = (1-x)\mu^{500C}_{\parallel,\perp}(E) + x\mu^{ox}(E) \quad (1)$$

where $\mu^{ox}(E)$ is one of the spectra collected on the oxides reference compounds (ox = CoO, Co_3O_4 or Co_{aq}). In the fits, the refined parameter x represents the fraction of oxidised Co suppressed by the second annealing. Assuming that after the 500 °C treatment, the films are made up only of Co^0, x represents the fraction of oxidised Co, while $1-x$ is the fraction of metallic Co. The fits obtained using $\mu_{ox} = Co_{aq}$ show the best agreement to the data for all the samples/polarizations. This points out to the presence of a highly disordered Co oxide phase, while Co_3O_4 or CoO occurrence can be considered negligible. This is compatible with the formation of a thin, disordered layer (CoO_{dis}) during the exposure to ambient pressure. For both the samples, the fractions of CoO_{dis} fitting $\mu^{300C}_{\perp}(E)$ and $\mu^{300C}_{\parallel}(E)$ are equal within the errors (see Tab.1). On the basis of the Co 2p XPS spectra collected *in-situ* (Fig.S1), no Co-oxide phases were present after Co deposition and intercalation, leaving the exposure to ambient pressure as the only possible cause for the Co-oxide formation. It is worthwhile noticing that the peak in the A region could be associated with Co-Ir intermixing [21] . However, as the intermixing is expected to increase with the temperature, the decrease of this peak upon the 500 °C treatment rules out this hypothesis.

	Thick film	**Thin film**
$CoO_{dis,\perp}$	16 ± 1 %	6 ± 2 %
$CoO_{dis,\parallel}$	16 ± 1 %	6 ± 2 %

Table 1: Amount of CoO_{dis} evaluated from the best fits of Fig. 3.

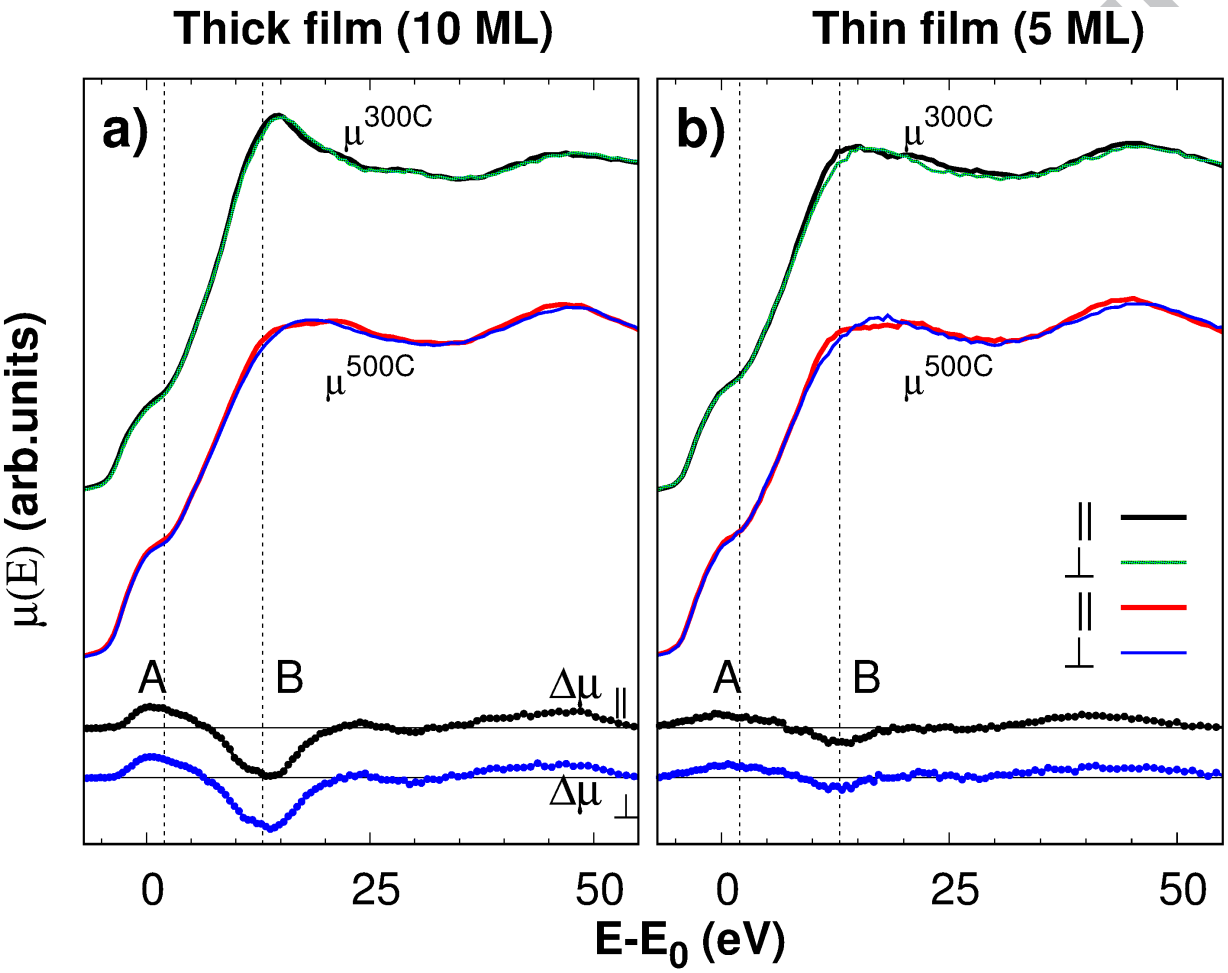

Figure 2: Normalized Co K-edge XANES of the thick (**a**) and thin (**b**) films. The top spectra, μ^{300C}, were collected after the 300°C annealing followed by exposure to ambient pressure for about 15 min. The bottom spectra, μ^{500C}, were measured after a second annealing at 500°C followed by another air exposure. In-plane (||) and out-of-plane (⊥) polarization geometries are shown. In the bottom part of each panel, the difference $\Delta\mu = \mu^{300C} - \mu^{500C}$ is reported for each polarization.

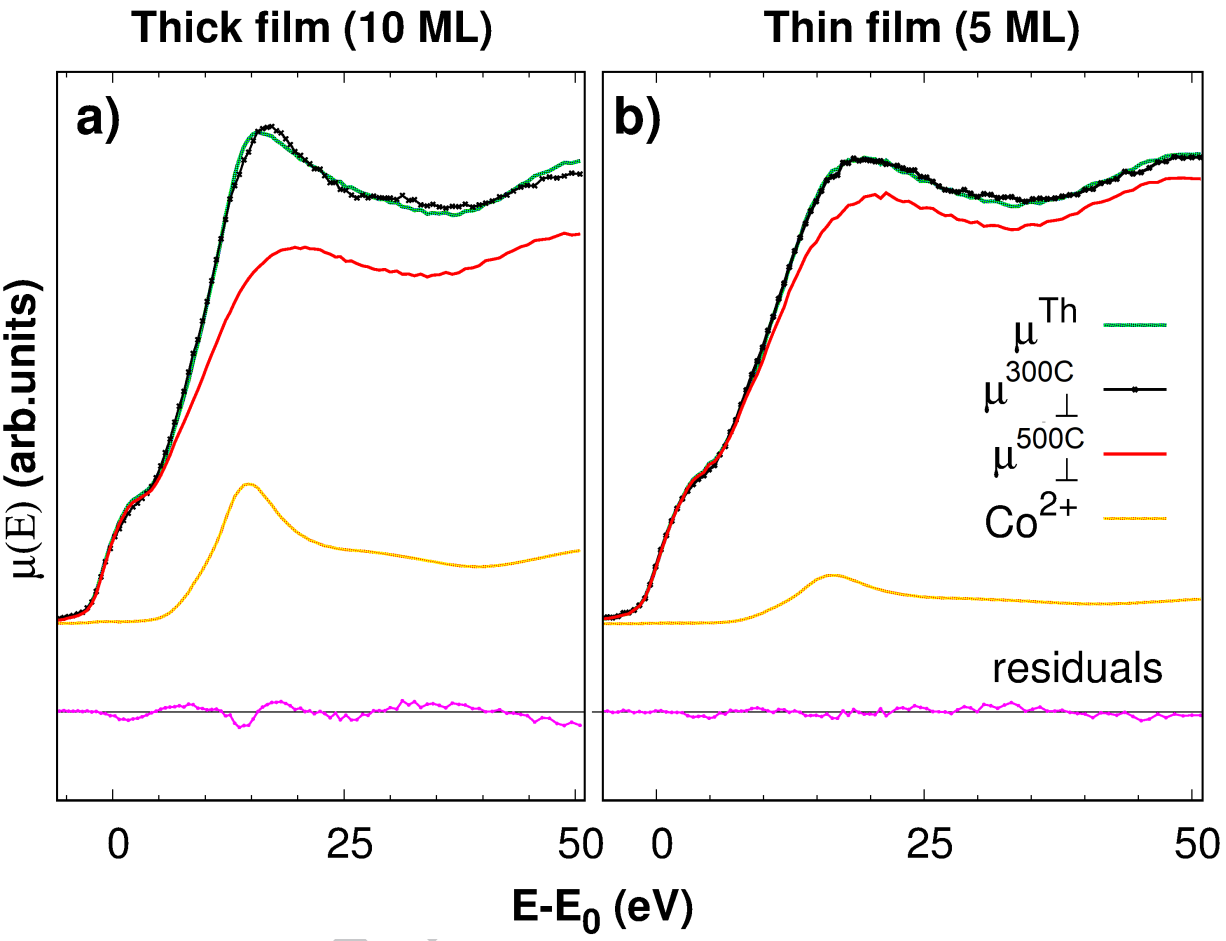

Figure 3: The experimental $\mu_{\perp}^{300C}(E)$ data (black dots) for **a)** the thick, and **b)** the thin films are presented together with the LCA best fits $\mu^{th}(E)$ (green lines). The weighted partial contributions used for LCA, $\mu_{\perp}^{500C}(E)$ and $\mu^{ox=Co_{aq}}$), are also reported. The residuals $\mu_{res}(E) = \mu_{\perp}^{300C}(E)$ - $\mu^{th}(E)$ are shown at the bottom.

In order to understand the origin of such oxidation we notice that if it were due to the inefficient protection offered by the Gr layer, the process would take place through the Gr itself, starting from the topmost region. Hence, a higher fraction of Co-oxide would be expected for thinner films, presenting a higher surface to volume ratio. Conversely, the data (Fig.2) and the LCA results (Fig.3 and Tab.1) depict the opposite trend, showing a higher CoO_{dis} contribution for the thick film. This suggests an incomplete intercalation leading to the oxidation of the Co atoms left on the Gr surface and indicates that the annealing time needed to achieve a complete intercalation depends on the amount of deposited Co. In fact, our thin sample is almost completely intercalated

while the thick one has a significant fraction of Co left on the Gr surface. Assuming a linear intercalation kinetics, we would expect about 50% of the Co in the thick film to oxidise. On the contrary, our findings suggest that the efficiency of the intercalation process for given annealing temperatures and times is thickness-dependent, increasing for thicker films.

The LCA results demonstrate that the amount of CoO_{dis} is reduced by the 500 °C thermal treatment. This finding together with the similarities in the $\mu^{500C}(E)$ spectra of thin and thick samples, suggests the full restoration of the metallic nature of both films and their full intercalation. The smearing of the XANES structural features with respect to metallic Co (Fig.S2) is known to originate from a major structural disorder [29]. Such effect can be due to the intrinsic nanostructured character of the film [19] and is enhanced in the perpendicular geometry, where the effects due to the disorder add up to that of the film thinness.

The oxide removal observed upon the 500 °C annealing cannot be ascribed to a straightforward CoO desorption mechanism, as this would cause a variation in the Co amount with a consequent reduction of the absorption edge jump. Moreover this effect would be higher for the thick film presenting the higher CoO fraction. On the contrary, comparing the raw data (shown after the pre-edge subtraction in Fig.4) no significant decrease of the edge jump is found upon the 500 °C annealing, pointing out how the reduction of oxidized phase occurs keeping constant the Co content. The CoO_{dis} phase dissociates during the 500 °C annealing and, while Oxygen atoms leave the sample, the Co remains. Co-oxide dissociation at 500 °C is an interesting finding as it generally requires higher temperatures ($T > 790$ °C [30]). It could be related to the combination of several factors such as: *i)* air exposure may cause humidity adsorption providing some OH functional groups favouring the dissociation; *ii)* it has been recently demonstrated that Co intercalation occurs through the Gr defects and Co atoms progressively diffuse below the Gr away from the intercalation site [31] while Oxygen tends to leave the Gr-covered regions [32]: hence the Gr may support the CoO dissociation and lower the reaction temperature (under H_2 flux, the reduction was observed at 500 °C [33, 34, 35]); *iii)* the freshly bound CoO_{dis} phase could interact weakly with the substrate, short exposure time, and substrate interactions as well as functional groups may have an important role on the degree of reducibility of CoO [33].

Interestingly, after the 500 °C annealing, both samples show negligible oxidation effects even

after air exposure (see μ^{500C} in Fig.2). This can be inferred from the similar shape of the two spectra, and is further confirmed upon comparison with the XANES data collected *in-situ* on Co/Ir systems [21]. The small anisotropy found around 15 eV above the edge for both samples supports the metallic, non-oxidised nature of the film despite the ambient pressure exposure performed after the 500 °C annealing [36]. The resistance to oxidation under atmospheric conditions is consistent with the complete intercalation of the Co below the Gr protective layer. It is worth noticing that the fraction of CoO_{dis} (Tab. 1) represents a tool to evaluate the efficiency of the intercalation procedure as a function of the film thickness and results to be 94% for the thin film and 84% for the thick film. This finding proves the thickness dependence of the intercalation process.

4. Conclusion

We have investigated the effectiveness of Co intercalation below Gr. Two films of 5 and 10 ML were intercalated between Gr and Ir(111) by annealing at 300 °C for 5 min. Upon 15 min of air exposure under ambient pressure, a disordered Co oxide phase was found on both the films, being more abundant in the thickest film. This has been interpreted as a sign of incomplete and thickness-dependent intercalation process. The disordered Co oxide was removed by annealing at 500 °C. A second exposure to air did not induce further oxidation, suggesting that a complete intercalation was achieved and demonstrating that completely intercalated Co films are protected against oxidation under atmospheric conditions for several minutes.

Acknowledgements

The authors wish to thank the staff of ID03 and BM23 beamlines, in particular, F. Carlà, T. Dufrane, H. Isern, S. Pascarelli, and O. Mathon for the scientific and technical support provided during the experiments.

[1] G. Avvisati, S. Lisi, P. Gargiani, A. Della Pia, O. De Luca, D. Pacile, C. Cardoso, D. Varsano, D. Prezzi, A. Ferretti, Fepc adsorption on the moiré superstructure of graphene intercalated with a cobalt layer, The Journal of Physical Chemistry C 121 (3) (2017) 1639–1647.

[2] J. Uihlein, H. Peisert, H. Adler, M. Glaser, M. Polek, R. Ovsyannikov, T. Chasse, Interface between fepc and ni (111): influence of graphene buffer layers, The Journal of Physical Chemistry C 118 (19) (2014) 10106–10112.

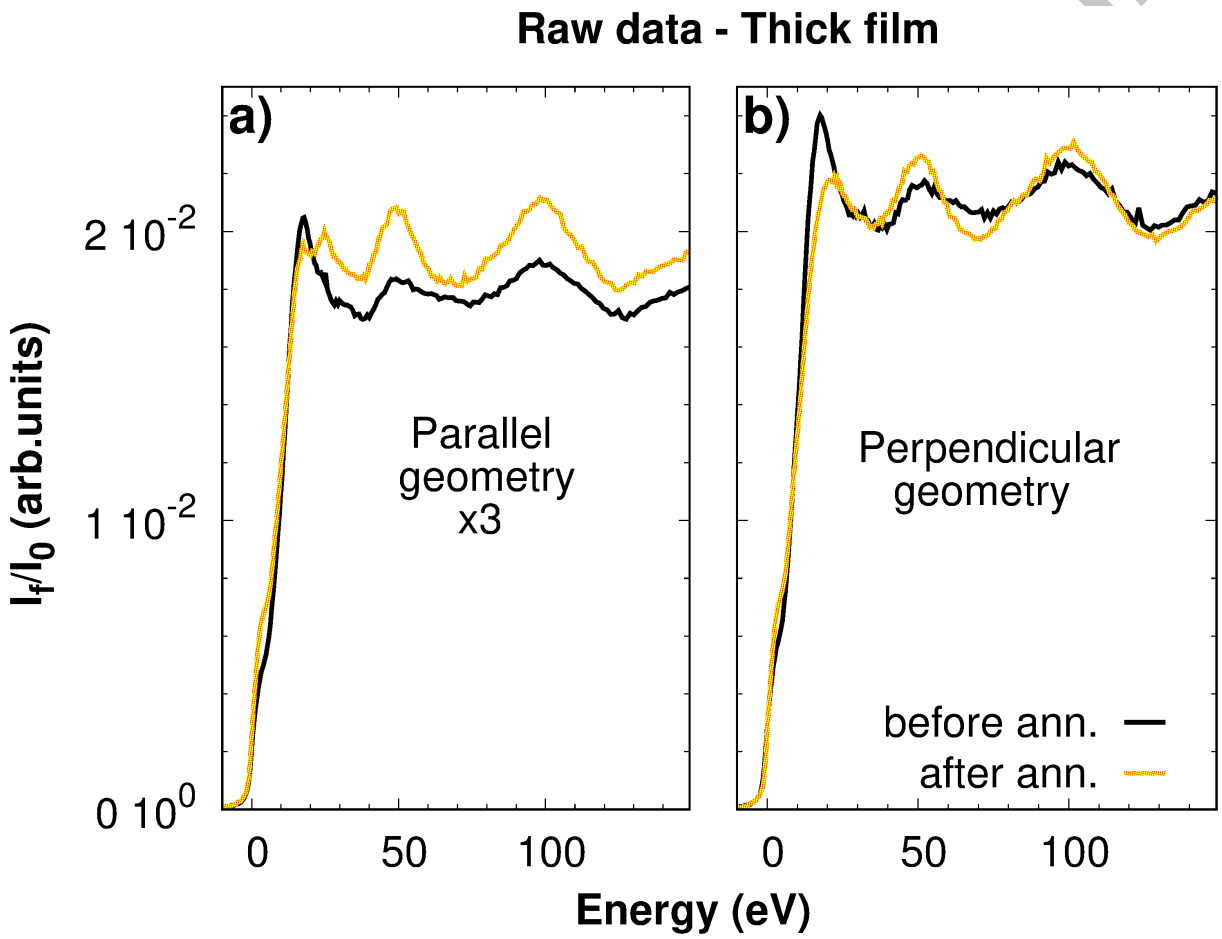

Figure 4: The raw normalized fluorescence data measured in **a)** parallel and **b)** perpendicular geometry for the thick film. The spectra are reported after the subtraction of the pre-edge background. The approximately equal edge jump discontinuity proves the negligible Co desorption upon annealing. The data collected in parallel geometry are less intense and have been multiplied by a factor of 3 for sake of comparison with panel b.

[3] N. Nishimura, T. Hirai, A. Koganei, T. Ikeda, K. Okano, Y. Sekiguchi, Y. Osada, Magnetic tunnel junction device with perpendicular magnetization films for high-density magnetic random access memory, J. Appl. Phys. 91 (2002) 5246.

[4] S. Ikeda, K. Miura, H. Yamamoto, K. Mizunuma, H. Gan, M. Endo, S. Kanai, J. Hayakawa, F. Matsukura, H. Ohno, A perpendicular-anisotropy *cofebmgo* magnetic tunnel junction, Nature Mat. 9 (2010) 721.

[5] A. Reina, X. Jia, J. Ho, D. Nezich, H. Son, V. Bulovic, M. Dresselhaus, J. Kong, Large area, few-layer graphene films on arbitrary substrates by chemical vapor deposition, Nano letters 9 (1) (2008) 30–35.

[6] L. G. De Arco, Y. Zhang, A. Kumar, C. Zhou, Synthesis, transfer, and devices of single-and few-layer graphene by chemical vapor deposition, IEEE Transactions on Nanotechnology 8 (2) (2009) 135–138.

[7] J. Coraux, M. Engler, C. Busse, D. Wall, N. Buckanie, F.-J. M. Zu Heringdorf, R. Van Gastel, B. Poelsema, T. Michely, Growth of graphene on ir (111), New Journal of Physics 11 (2) (2009) 023006.

[8] Y. S. Dedkov, M. Fonin, Electronic and magnetic properties of the graphene–ferromagnet interface, New Journal of Physics 12 (12) (2010) 125004.

[9] S. Schumacher, F. Huttmann, M. Petrović, C. Witt, D. Förster, C. Vo-Van, J. Coraux, A. J. Martínez-Galera, V. Sessi, I. Vergara, R. Rückamp, M. Grüninger, N. Schleheck, F. Meyer zu Heringdorf, P. Ohresser, M. Kralj, T. O. Wehling, T. Michely, Europium underneath graphene on ir(111): Intercalation mechanism, magnetism, and band structure, Phys. Rev. B 90 (2014) 235437.

[10] M. Petrović, I. Rakić, S. Runte, C. Busse, J. Sadowski, P. Lazić, I. Pletikosić, Z. Pan, M. Milun, P. Pervan, The mechanism of caesium intercalation of graphene, Nature communications 4.

[11] D. Pacilé, P. Leicht, M. Papagno, P. Sheverdyaeva, P. Moras, C. Carbone, K. Krausert, L. Zielke, M. Fonin, Y. Dedkov, F. Mittendorfer, J. Doppler, A. Garhofer, J. Redinger, Artificially lattice-mismatched graphene/metal interface: Graphene/ni/ir(111), Phys. Rev. B 87 (2013) 035420.

[12] H. Vita, S. Böttcher, K. Horn, E. Voloshina, R. Ovcharenko, T. Kampen, A. Thissen, Y. S. Dedkov, Understanding the origin of band gap formation in graphene on metals: graphene on cu/ir (111), Scientific Reports 4 (2014) 5704.

[13] J. Coraux, A. T. NDiaye, N. Rougemaille, C. Vo-Van, A. Kimouche, H. Yang, M. Chshiev, N. Bendiab, O. Fruchart, A. K. Schmid, Air-protected epitaxial graphene/ferromagnet hybrids prepared by chemical vapor deposition and intercalation, J. Phys. Chem. Lett. 3 (2012) 2059.

[14] H. Vita, S. Böttcher, P. Leicht, K. Horn, A. B. Shick, F. Máca, Electronic structure and magnetic properties of cobalt intercalated in graphene on ir(111), Phys. Rev. B 90 (2014) 165432.

[15] R. Decker, J. Brede, N. Atodiresei, V. Caciuc, S. Blügel, R. Wiesendanger, Atomic-scale magnetism of cobalt-intercalated graphene, Phys. Rev. B 87 (2013) 041403.

[16] D. Pacilé, S. Lisi, I. Di Bernardo, M. Papagno, L. Ferrari, M. Pisarra, M. Caputo, S. K. Mahatha, P. M. Sheverdyaeva, P. Moras, P. Lacovig, S. Lizzit, A. Baraldi, M. G. Betti, C. Carbone, Electronic structure of

graphene/co interfaces, Phys. Rev. B 90 (2014) 195446.

[17] S. Vlaic, A. Kimouche, J. Coraux, B. Santos, A. Locatelli, N. Rougemaille, Cobalt intercalation at the graphene/iridium(111) interface: Influence of rotational domains, wrinkles, and atomic steps, Appl. Phys. Lett. 104 (2014) 101602.

[18] A. Vu, J. Coraux, G. Chen, A. NDiaye, A. Schmid, N. Rougemaille, Unconventional magnetisation texture in graphene/cobalt hybrids, Scientific reports 6 (2016) 24783.

[19] J. Drnec, S. Vlaic, I. Carlomagno, C. J. Gonzalez, H. Isern, F. Carlà, R. Fiala, N. Rougemaille, J. Coraux, R. Felici, Surface alloying upon co intercalation between graphene and ir (111), Carbon 94 (2015) 554.

[20] W.-Y. Chan, D.-C. Tsai, W.-H. Chen, J.-S. Tsay, Enhancement of the polar coercive force for annealed co/ir (111) ultrathin films, Journal of the Korean Physical Society 62 (12) (2013) 1945–1949.

[21] I. Carlomagno, J. Drnec, A. Scaparro, S. Cicia, S. Vlaic, R. Felici, C. Meneghini, Co-ir interface alloying induced by thermal annealing, Journal of Applied Physics 120 (19) (2016) 195302.

[22] N. Rougemaille, A. N'Diaye, J. Coraux, C. Vo-Van, O. Fruchart, A. Schmid, Perpendicular magnetic anisotropy of cobalt films intercalated under graphene, Appl. Phys. Lett. 101 (2012) 142403.

[23] P. Guntera, O. Gijzemanb, J. Niemantsverdriet, Surface roughness effects in quantitative xps: magic angle for determining overlayer thickness, Appl. Surf. Sci. 115 (1997) 342.

[24] C. Fadley, Electron Spectroscopy: Theory, Techniques and Applications, Vol. 2, Academic Press, 1978, Ch. Basic concepts of XPS.

[25] G. Bunker, Introduction to XAFS, Cambridge University Press, 2010.

[26] C. Meneghini, S. Di Matteo, C. Monesi, T. Neisius, L. Paolasini, S. Mobilio, C. Natoli, P. Metcalf, J. Honig, Antiferromagnetic paramagnetic insulating transition in cr-doped v_2o_3 investigated by exafs analysis, J. Phys. Condens. Matter 21 (2009) 355401.

[27] F. Liscio, M. Maret, C. Meneghini, S. Mobilio, O. Proux, D. Makarov, M. Albrecht, Structural origin of perpendicular magnetic anisotropy in epitaxial $copt_3$ nanostructures grown on $wse_2(0001)$, Phys. Rev. B 81 (2010) 125417.

[28] C. Meneghini, M. Benfatto, Synchrotron Radiation, Springer, 2016, Ch. VII.

[29] M. Farges, G. E. Brown, J. J. Rehr, Ti k-edge xanes studies of ti coordination and disorder in oxide compounds: Comparison between theory and experiment, Phys. Rev. B 56 (1997) 1809–1819.

[30] J. Yang, H. Liu, W. N. Martens, R. L. Frost, Synthesis and characterization of cobalt hydroxide, cobalt oxyhydroxide, and cobalt oxide nanodiscs, The Journal of Physical Chemistry C 114 (1) (2010) 111–119. doi:10.1021/jp908548f.

[31] S. Vlaic, N. Rougemaille, A. Kimouche, B. S. Burgos, A. Locatelli, J. Coraux, Intercalating cobalt between graphene and iridium (111): Spatially dependent kinetics from the edges, Physical Review Materials 1 (5) (2017) 053406.

[32] E. Gránäs, J. Knudsen, U. A. Schrder, T. Gerber, C. Busse, M. A. Arman, K. Schulte, J. N. Andersen, T. Michely, Oxygen intercalation under graphene on ir(111): Energetics, kinetics, and the role of graphene edges, ACS Nano (2012) 9951–9963.

[33] S. Taghavi, A. Asghari, A. Tavasoli, Enhancement of performance and stability of graphene nano sheets supported cobalt catalyst in fischer–tropsch synthesis using graphene functionalization, Chemical Engineering Research and Design 119 (2017) 198–208.

[34] S. Karimi, A. Tavasoli, Y. Mortazavi, A. Karimi, Cobalt supported on graphene–a promising novel fischer–tropsch synthesis catalyst, Applied Catalysis A: General 499 (2015) 188–196.

[35] J. Moon, K. Park, J. Kim, G. Seo, Reductive removal of dissolved oxygen in water by hydrazine over cobalt oxide catalyst supported on activated carbon fiber, Applied Catalysis A: General 201 (1) (2000) 81–89.

[36] N. Marsot, R. Belkhou, H. Magnan, P. Le Fèvre, C. Guillot, D. Chandesris, Structure and local order in co magnetic thin films on au(111): A surface exafs study, Phys. Rev. B 59 (1999) 3135–3141.

Highlights

- The intercalation of Co films through defective Graphene is thickness dependent
- Non-intercalated Co forms a disordered CoO phase under ambient pressure exposure
- The oxide phase can be used to evaluate the amount of non-intercalated Co
- Further annealing induces the oxide reduction to metallic Co and its intercalation
- The intercalated Co is prevented from oxidation upon ambient pressure exposure

Graphical Abstract